ACS APPLIED MATERIALS & INTERFACES

Research Article

www.acsami.org

Graphene Networks with Low Percolation Threshold in ABS Nanocomposites: Selective Localization and Electrical and Rheological Properties

Chong Gao,[†,‡] Shimin Zhang,[†] Feng Wang,[†] Bin Wen,[†] Chunchun Han,[†,‡] Yanfen Ding,[†] and Mingshu Yang*[,†]

[†]Beijing National Laboratory for Molecular Sciences, Key Laboratory of Engineering Plastics, Institute of Chemistry, Chinese Academy of Sciences, Zhongguancun North First Street 2, Beijing 100190, P. R. China

[‡]University of Chinese Academy of Sciences, Beijing, 100049, P. R. China

ABSTRACT: Acrylonitrile-butadiene-styrene resin (ABS)/graphene nanocomposites were prepared through a facile coagulation method. Because the chemical reduction of graphene oxide was in situ conducted in the presence of ABS at the dispersion stage, the aggregation of the graphene nanosheets was avoided. It was shown by transmission electron microscopy that the graphene nanosheets were selectively located and homogeneously dispersed in the styrene-acrylonitrile (SAN) phase. The electrical conductivity and linear viscoelastic behavior of the nanocomposites were systematically studied. With increasing filler content, graphene networks were established in the SAN phase. Consequently, the nanocomposites underwent a transition from electrical insulator to conductor at a percolation threshold of 0.13 vol %, which is smaller than that of other ABS composites. Such a low percolation threshold results from extreme geometry, selective localization, and homogeneous dispersion of the graphene nanosheets in SAN phase. Similarly, the rheological response of the nanocomposites also showed a transition to solid-like behavior. Due to the thermal reduction of graphene nanosheets and structure improvement of graphene networks, enhanced electrical conductivity of the nanocomposites was obtained after annealing.

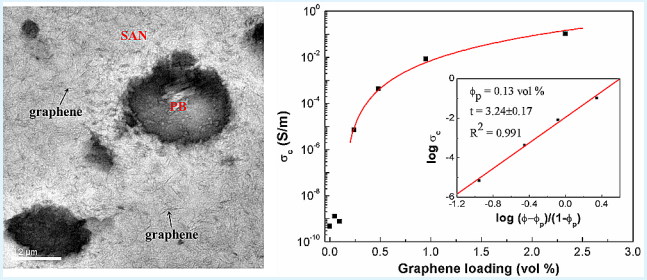

KEYWORDS: *ABS resin, graphene, network, selective localization, electrical conductivity, rheology*

1. INTRODUCTION

It is well-known that polymer composites containing conductive fillers, such as carbon nanotube (CNT),[1] carbon fiber,[2] and carbon black (CB),[3] become conductive when the filler loading exceeds a critical value, named percolation threshold in terms of percolation theory,[4,5] due to the formation of conductive networks. Depending on the geometric structure and dispersion of the fillers, the conductive networks establish in a wide concentration range. Du et al. prepared poly(methyl methacrylate) (PMMA)/multiwall carbon nanotube (MWNT) composites with a low electrical percolation threshold of 0.39 wt %.[6] In contrast, PMMA/CB composites exhibit a percolation value of 13.0 wt %.[3] Unfortunately, large contents of conductive fillers usually lead to poor processability and mechanical performance. In order to preserve the mechanical properties and processing ease of the composites, a low percolation threshold is indispensable. Ongoing studies on formation of the conductive networks have demonstrated that addition of the conductive fillers with large aspect ratio, such as fibers and sheets, and to locate the fillers in one polymer phase or even better at the interphase of the immiscible blends are pretty effective strategies.[7−17]

The aspect ratio of the fillers is the most important factor affecting the percolation threshold. Irrespective of the entanglement of the fillers, the percolation threshold would decrease with increasing aspect ratio. The positive effect of aspect ratio can be explained by the excluded volume theory.[7−9] The excluded volume is defined as the volume around an object into which the center of another similar object is not allowed to enter if interpenetration of the two objects is to be avoided. In case that the actual volume of the object is invariant, the higher aspect ratio induces the larger excluded volume, and thus lowers the percolation threshold. In fact, Bai et al. reported a decrease of percolation threshold from 4 to 0.5 wt % relating to an increase of the CNT aspect ratio from 8 to 420.[10] Li et al. also proposed that if the CNT aspect ratio is too low a very high CNT content is needed to form the conductive networks, no matter how the CNT dispersion state is.[11]

Graphene, which was experimentally prepared by Novoselov et al. at the earliest in 2004, is a two-dimensional monolayer or few-layer carbon material.[18] It has attracted enormous attention

Received: March 27, 2014
Accepted: June 27, 2014
Published: June 27, 2014

due to its excellent mechanical, thermal, electrical properties, and large aspect ratio. The extreme geometry of graphene makes it favorable to form networks at low filler content. To date, various polymer/graphene conductive nanocomposites have been reported. Using coagulation method, PS/graphene nanocomposites were prepared by Stankovich et al., and exhibited a very low electrical conductivity percolation threshold of ∼0.1 vol %.[19] Graphene nanosheets begin to form conductive networks in polyethylene terephthalate (PET)/graphene nanocomposites at a critical value of 0.47 vol %, much lower than that in PET/graphite composites at 2.4 vol %.[20]

Another practical method to lower the electrical percolation threshold is to incorporate conductive fillers into immiscible polymer blends. In this case, the electrical conductivity predominantly depends on the morphology of the blend and distribution of the filler, which relies on the affinity of the filler to the polymers, the processing history, and the post-treatment. When the filler preferentially resides in one phase or at the interphase of the blend, meanwhile the filler-rich phase is continuous throughout the polymer blend, the percolation threshold would appear a low value. This has been called double percolation phenomenon, i.e., filler percolation and phase percolation.[13] Gubbels et al. prepared cocontinuous polyethylene (PE)/polystyrene (PS) blends in which CB particles tended to localize in the PE phase.[14,15] Compared with the percolation threshold of 8 wt % for PS/CB and 5 wt % for PE/CB, the blends showed a lower critical value of 3 wt %. Since the interactions between the CB surface and the polymers were weak and nearly identical, the CB particles were located at the interphase of the blends after a post-treatment. Consequently, the percolation threshold was further reduced to 0.4 wt %, due to the decrease of the tortuosity of the polymer phases and the interphase area after the post-treatment. Qi et al. reported that graphene nanosheets selectively localized in PS phase after PS/graphene nanocomposites were incorporated with PLA, accordingly, resulting in a decrease of percolation threshold from ∼0.33 to ∼0.075 vol %.[16]

No matter from applied or theoretical points of view, rheological properties of composites are very important. Rheological methods have been widely used to study polymer composites, since the viscoelastic behavior is highly sensitive to the microstructure of the composites melt, the dispersion state of fillers, and the interactions between fillers and polymer matrices. In the linear viscoelastic regime, where the structure of the material is supposed to remain almost unchanged, the incorporation of fillers makes a great impact on the viscoelastic properties, including storage modulus G', loss modulus G'', complex viscosity η^*, and loss tangent tan δ, especially in low frequency range. Solomon et al. reported that polypropylene/clay hybrid materials exhibited apparent low-frequency plateaus in the linear storage modulus when the inorganic loading was 2.0 wt % or more.[21] Ren et al. observed a transition to solid-like behavior at low frequencies in polystyrene−polyisoprene block copolymer based layered-silicate nanocomposites.[22] Many other researchers also reported this nonterminal viscoelastic rheological behavior in polymer composites incorporated with other fillers, such as CNT,[6] graphene,[23] and so on. This nonterminal solid-like behavior has been attributed to the percolated filler networks, penetrating throughout the polymer matrix.

Acrylonitrile-butadiene-styrene resin (ABS), consisting of styrene-acrylonitrile copolymer (SAN) phase and polybutadiene (PB) phase with sea−island structure, is a widely used thermoplastic copolymer, due to its excellent mechanical properties and chemical resistance. Electrically conductive blends of ABS and other polymers with selective localization of fillers have been reported, exhibiting excellent electrical properties in contrast to the composites with single polymer phase.[24,25] However, to our knowledge, few works on the selective localization of fillers in the SAN phase are reported. This work is aimed to prepare ABS/graphene nanocomposites with selective localization of graphene in SAN phase through a facile coagulation method. The dispersion of graphene nanosheets in the nanocomposites and electrical and rheological properties of the nanocomposites were systematically examined. The influence of thermal annealing on electrical properties of the nanocomposites was also investigated.

2. EXPERIMENTAL SECTION

2.1. Materials. Natural flake graphite (NG) with an average size of 180 μm and a purity of >99% was supplied by Beijing Invention Biology Engineering & New Material Co., Ltd., China. Acrylonitrile-butadiene-styrene resin (ABS), a commercial product (PA-757 K) consisting of 21.0 vol % (∼19.5 wt %) SAN-grafted PB rubber, was obtained from Zhenjiang Chi Mei Chemical Co., Ltd., China. The T_g of SAN phase and PB rubber are +111.6 and −80.9 °C, respectively. Potassium permanganate ($KMnO_4$, AR − analytical reagent grade), sodium nitrate ($NaNO_3$, AR), hydrogen peroxide (H_2O_2, 30% aq.), sulfuric acid (H_2SO_4, 98%), hydrochloric acid (HCl, 35% aq.), barium chloride ($BaCl_2$, AR), hydrazine hydrate ($N_2H_4{\cdot}H_2O$, 80% aq.), and dimethylformamide (DMF, AR) were all used as received.

2.2. Preparation of Graphite Oxide and Graphene Oxide Nanosheets. Graphite oxide (GO) was prepared by a modified Hummers method from natural flake graphite.[26] Typically, 8 g of graphite and 6 g of $NaNO_3$ were mixed with 600 mL of H_2SO_4 in a flask under vigorous stirring in an ice bath. When the mixture cooled to 3−4 °C, 36 g of $KMnO_4$ was added slowly within 0.5 h while keeping the temperature of the mixture below 10 °C. After it was stirred for another 2.5 h, the mixture was moved into a water bath at 35 °C and maintained for 24 h. Then, 1200 mL of deionized water was dripped into the flask in 1 h, causing an increase of temperature to 96−98 °C. After the mixture cooled to 60 °C under ambient condition, 80 mL of H_2O_2 was added. Finally, the resultant mixture was filtered and washed with dilute HCl until no sulfate could be detected by $BaCl_2$ solution, followed by dialysis in deionized water for one month. GO was collected after dried in vacuum oven at 60 °C for 24 h before use.

The dried GO was dispersed in DMF. Stable suspension of graphene oxide nanosheets in DMF was prepared through ultrasonic exfoliation of GO under a power of 300 W for 2 h.

2.3. Preparation of ABS/Graphene Nanocomposites. Coagulation method was applied to prepare the ABS/graphene nanocomposites. Briefly, ABS particles were added into the suspension of graphene oxide nanosheets in DMF under stirring. After ABS was dissolved, reduction of graphene oxide was performed with $N_2H_4{\cdot}H_2O$ (the weight ratio of $N_2H_4{\cdot}H_2O$ to graphene oxide was 1:1) under stirring at 90 °C for 4 h. Afterward, the admixture was gradually poured into a stirring bath containing large volume of deionized water, and the nanocomposite was coagulated and precipitated. The precipitate was filtered, washed repeatedly with deionized water, and finally dried in vacuum oven at 80 °C for ∼24 h. Testing specimens of the ABS/graphene nanocomposites were prepared by compression molding in a vacuum hydraulic hot press at 10 MPa and 210 °C with a fixed dwell time of 10 min. Disk specimens (Φ25 mm × 1 mm) were used for rheology tests and rectangle ones (20 mm × 15 mm × 1 mm) for resistance measurements. Thermal annealing treatment of the specimens was conducted at 210 °C under 10 MPa for varied time. To convert loading of graphene from weight to volume fraction, the density used here is of 2.2 g/cm^3 for graphene and 1.05 g/cm^3 for ABS.

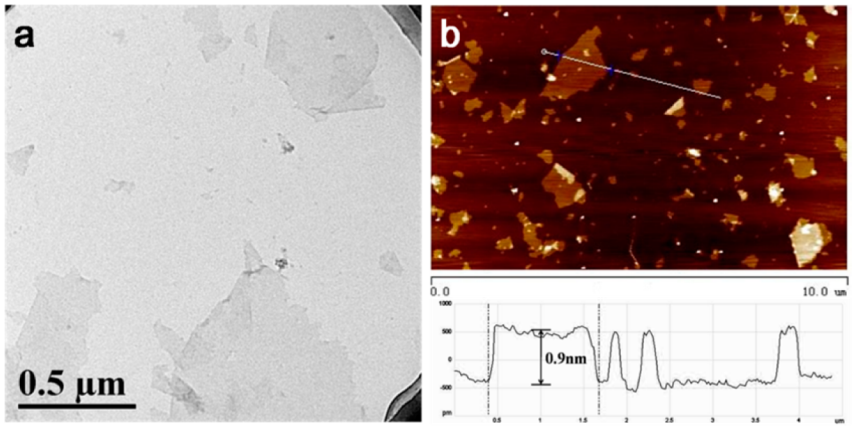

Figure 1. TEM (a) and AFM (b) micrographs of graphene oxide nanosheets.

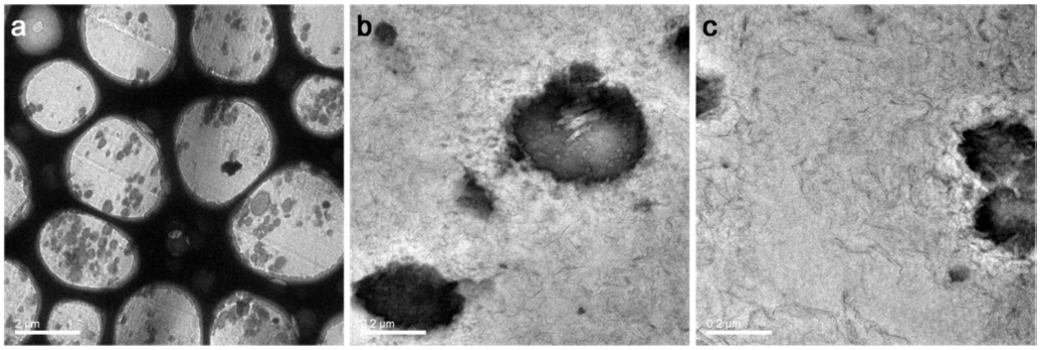

Figure 2. TEM micrographs of ABS nanocomposite with 2.33 vol % graphene loading: (a) low magnification (the irregular circles with diameter of ca. 2 μm are the micropores of carbon film on the copper grids) and (b, c) high magnification. The black granules are the PB phase islands.

2.4. Characterization. Transmission electron microscopy (TEM, JEM-2100, JEOL, Japan) was used to characterize the microstructure of graphene oxide nanosheets and the dispersion of graphene in the ABS nanocomposites. Graphene oxide suspension was dripped onto copper grids for observation. The ABS nanocomposites were cryogenically cut into ultrathin sections using a Leica microtome at −100 °C, collected to copper grids, and stained with 1.0 wt % OsO_4 aqueous solution at 25 °C for 8 h.

Atomic force microscopy (AFM) images were obtained using a DI Multimode 8 scanning probe microscope from Bruker Corporation of Germany. The microstructure of graphene oxide nanosheets was observed in tapping mode under ambient conditions at a scanning rate of 1 Hz. Samples for AFM images were prepared by dripping graphene oxide suspension onto a freshly cleaved mica surface, allowing free evaporation of the solvent in the open air.

Rheological measurements were performed at 210 °C on a stress-controlled rheometer (AR2000 ex, TA Instruments, USA) equipped with Φ25 mm parallel plate geometry and 1 mm sample gap. The sample chamber was purged by a continuous flow of nitrogen gas in order to avoid degradation of the nanocomposites. To determine the linear viscoelastic regime, strain sweep experiments were carried out at an angular frequency of 1 rad/s. Based on the results, an appropriate strain amplitude of 0.3% was applied for oscillatory frequency sweep from 0.02 to 200 rad/s.

The direct current resistance of the nanocomposites was measured by a semiconductor characterization system (Keithley 4200-SCS, Keithley Instruments Inc., USA) using the two-probe method at room temperature. Before testing, silver paste was coated on the two ends of the sample to reduce the contact resistance between the samples and the probes. The electrical conductivity σ was obtained from eq 1:

$$\sigma = \frac{1}{\rho} = \frac{d}{RS} \quad (1)$$

where ρ is the electrical resistivity, d the thickness of the samples, R the electrical resistance, and S the cross section area of the sample.

X-ray photoelectron spectroscopy (XPS) measurements were conducted by an ESCALab220i-XL electron spectrometer from VG Scientific with 300W Al Kα radiation. The base pressure was about 3×10^{-9} mbar. The binding energies were referenced to the C 1s line at 284.8 eV from adventitious carbon. XPSpeak 3.01 software was used to resolve overlapping peaks and to calculate the atomic concentration ratio.

3. RESULTS AND DISCUSSION

3.1. Characterization of Graphene Oxide Nanosheets. TEM and AFM images of graphene oxide nanosheets are shown in Figure 1. Apparently, both of the images showed the ultrathin thickness and the wide size distribution of graphene oxide nanosheets prepared in this research. AFM image of graphene oxide nanosheets displayed a height of ∼0.9 nm, which is much larger than the theoretical height of 0.335 nm of graphene. The oxygen-containing groups on the surface of graphene oxide nanosheets are responsible for the larger height. Both the TEM and AFM images suggest the full exfoliation of GO in the ultrasonically treated dispersion.

3.2. Dispersion of Graphene Nanosheets in the Nanocomposites. ABS/graphene nanocomposites were prepared through coagulation method, which may make graphene nanosheets distributed mainly in the SAN phase since the rubber phase is insoluble in DMF. In order to clearly observe the dispersion of graphene nanosheets, TEM was carried out for the nanocomposite. As shown in Figure 2a, the stained PB granules were interspersed in the SAN phase, and no graphene aggregates were observed. In Figure 2b,c, the dark lines are the

cross sections of graphene nanosheets. The wrinkled graphene nanosheets were homogeneously dispersed throughout the SAN phase, which suggests that the SAN chains had effectively prevented the aggregation of graphene nanosheets during reduction. Besides, it is difficult to see any graphene nanosheets in the PB phase; that is to say, most graphene nanosheets were selectively located in the SAN phase. It has been reported that a strong $\pi-\pi$ stacking interaction exists between aromatic organic molecules and the basal plane of graphite.[27] The interaction can prevent graphene from aggregation during chemical reduction and migration from the SAN phase which contains aromatic phenyl groups to the PB phase during hot-compression. Therefore, the excellent dispersion and selective localization of graphene nanosheets should be attributed to the preparation method and the strong $\pi-\pi$ interaction between graphene and the phenyl rings of SAN chains. In addition, it was found that continuous graphene networks were formed in the matrix, providing pathways for electron transportation, as discussed later in detail.

3.3. Electrically Conductive Networks. As mentioned above, the conductivity transition for polymer composites is a consequence of the formation of conductive networks. At low loading, the graphene nanosheets disperse separately from each other in the SAN phase. With increasing the graphene content to exceed the percolation threshold, lots of graphene nanosheets get close enough to each other to form conductive paths for electron hopping, and then networks throughout the matrix for electron transportation.

Figure 3a displays the electrical conductivity dependence on graphene loading for the ABS/graphene nanocomposites. It is evidenced that the electrical conductivity strongly depended on the graphene content. At the graphene content of 0.24 vol %, the conductivity was 7.1×10^{-6} S/m, which already exceeds the common antistatic criterion 10^{-6} S/m. With an increase of graphene loading to 0.48 vol %, the electrical conductivity quickly rose to 4.3×10^{-4} S/m. Above 0.48 vol %, it showed a gradual increase with 8.5×10^{-3} S/m at 0.95 vol % and 0.1 S/m at 2.33 vol %.

Above the percolation threshold, the electrical conductivity of the nanocomposites σ_c can be treated with the power law:

$$\sigma_c = \sigma_f[(\varphi - \varphi_p)/(1 - \varphi_p)]^t \text{ for } \varphi > \varphi_p \quad (2)$$

where σ_f is the conductivity of the filler, φ the filler volume fraction, φ_p the percolation volume fraction, and t the universal critical exponent revealing the dimensionality of the conductive networks.[19,28] The linear fit to the log–log plot of conductivity versus $(\varphi - \varphi_p)/(1 - \varphi_p)$ (inset in Figure 3a) resulted in φ_p = 0.13 vol %, $\sigma_f = 10^{4.53\pm0.39}$ S/m, and $t = 3.24 \pm 0.17$. To the best of our knowledge, the percolation threshold obtained here is one of the lowest values for ABS composites incorporated with various fillers.[29−33] In comparison, SAN/graphene nanocomposites were prepared through the same method. As shown in Figure 3b, the electrical conductivity of SAN/graphene nanocomposites exhibited a higher percolation threshold of 0.17 vol %. It indicates that the selective localization of graphene nanosheets does make contribution to lowering the percolation threshold. The percolation threshold of graphene nanosheets in SAN phase of ABS was calculated through division of the threshold in ABS resin 0.13 vol % by the content of SAN phase 79.0 vol %. As a result, a value of 0.16 vol % was obtained, which was in accordance with that in SAN/graphene nanocomposites. This confirms the selective localization of graphene in SAN phase indirectly. Such a low percolation threshold is believed to be derived from the extreme geometry, excellent dispersion, and selective localization of the graphene nanosheets in SAN phase.

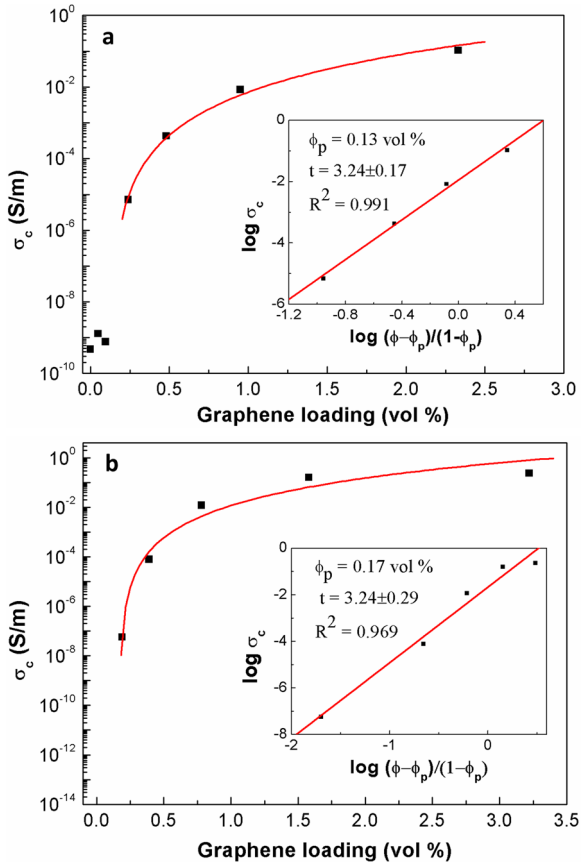

Figure 3. Electrical conductivity σ_c of the ABS/graphene nanocomposites (a) and SAN/graphene nanocomposites (b) as a function of graphene loading. The insets are log–log plots of σ_c versus $(\varphi - \varphi_p)/(1 - \varphi_p)$.

The t value of three-dimensional (3D) random percolation has been predicted in the range of 1.5 to 2.0, which is accepted as a universal value.[34] However, a higher value of t (3.24) for ABS/graphene nanocomposites was obtained here, as previously reported 2.74 for PS/graphene,[19] 4.22 for PET/graphene,[20] 4.18 and 4.04 for PC/graphene,[35] and 3.47 for PMMA/graphite nanosheets,[36] displaying nonuniversality. It has been demonstrated that the t values are higher for the conductive fillers with extreme geometry.[4,34] Supposing that graphene nanosheets can be regarded as disks with average diameter D and thickness h, the average aspect ratio A_f of graphene nanosheets, which is defined as the ratio of D to h, can be calculated by the following equation:[37]

$$A_f = \frac{D}{h} = \frac{3\varphi_{sphere}}{2\varphi_p} \quad (3)$$

where φ_{sphere} = 0.29 is the percolation threshold of random packed 3D interpenetrating spheres[37,38] and φ_p here is the conductive percolation threshold of graphene nanosheets in SAN phase. As a result, an average aspect ratio of approximate 272 was obtained for the graphene nanosheets prepared in this work. Such a great aspect ratio leads to the higher value of t and a different transport behavior.

3.4. Rheological Networks. It has been mentioned that, in the linear viscoelastic regime, the filler networks can be detected through the variation of the complex viscosity η^*, storage modulus G', loss modulus G'', and loss tangent tan δ with frequency. In order to elucidate the formation of graphene networks in the ABS matrix, the dynamic oscillatory rheology properties of the nanocomposites melt were characterized at 210 °C.

For determining the linear viscoelastic regime, strain sweep experiments were performed at an angular frequency of 1 rad/s for all the nanocomposites. Figure 4 depicts the storage modulus G' as a function of strain amplitude γ. In the low strain range, G' showed no strain-dependence, revealing a linear viscoelastic regime. Whereas with increasing strain, a pronounced reduction of G' was observed, which is known as Payne effect in the filled elastomer systems.[39,40] Payne effect, which has been studied extensively in the recent years, was mainly explained by the breakdown of the filler networks formed in the matrix above the percolation threshold.[41] For the ABS/graphene nanocomposites in our work, the existence and breakage of graphene networks at high loadings is responsible for the nonlinearity of G' at large deformation. With increasing strain, the graphene networks were destroyed, resulting in the decline of G'. The critical strain (γ_c), defining the boundary of the linear viscoelastic regime, was determined by calculating where G' deviates 10% from the plateau. The higher graphene loading is, the more complete the graphene networks form. Consequently, the γ_c value showed a shift toward lower values as graphene content increased. The dependence of γ_c on graphene loading is plotted in the inset of Figure 4. It is clear that the value of γ_c was almost unchanged at very low loading of graphene (0.048 vol %), whereas with increasing graphene content, a rapid decline of γ_c before 0.24 vol % and a moderate decline after 0.24 vol % appeared successively. This is similar to the tendency of electrical conductivity dependence on graphene loading, indicative of the network percolation behavior.

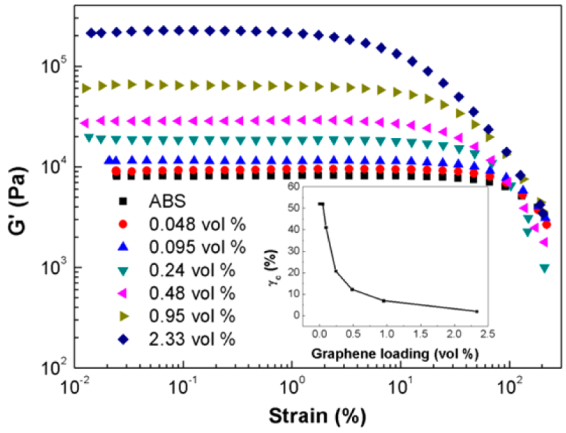

Figure 4. Storage modulus G' of ABS and its graphene nanocomposites as a function of strain amplitude at 210 °C. The inset is the plot of critical strain γ_c versus graphene loading.

Based on the results obtained from the strain sweeps, frequency sweeps were performed at a strain amplitude of 0.3% from 0.02 rad/s to 200 rad/s. Figure 5 gives the dependence of storage modulus G' and loss modulus G'' on angular frequency ω for the pure ABS and its nanocomposites. By comparison with the linear viscoelastic response of the pure ABS, a substantial effect of graphene nanosheets was evidenced in the nanocomposites. With increasing graphene content, both G' and G'' of the nanocomposites were significantly enhanced and became less dependent on ω throughout the test range. The diminished dependence on ω indicates that the nanocomposites gradually showed solid-like behavior, which is attributed to the formation of graphene networks.[42,43]

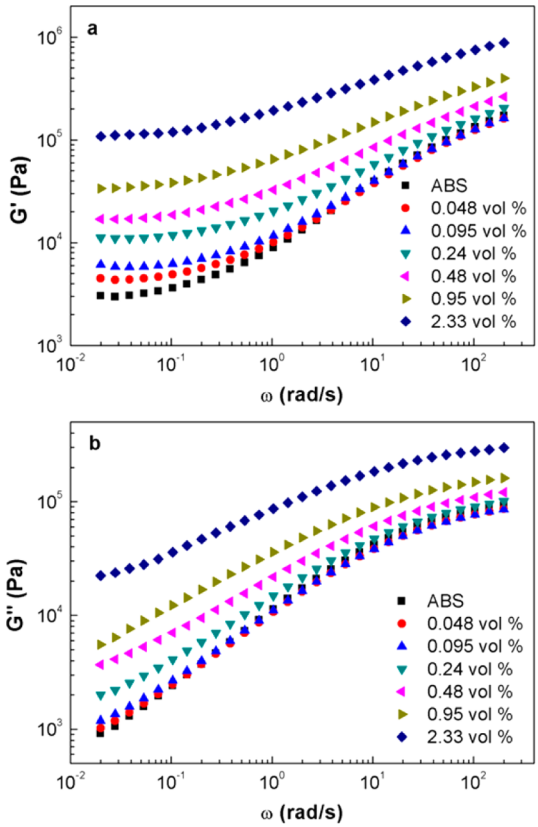

Figure 5. Storage modulus G' (a) and loss modulus G'' (b) of ABS and its graphene nanocomposites as a function of angular frequency ω at 210 °C.

It is obvious that, in the low frequency regime, a plateau in G'-ω plot was approached for all the samples, indicative of nonterminal behavior. And with increasing graphene content, the plateau extended to a higher ω. Namely, the nonterminal behavior became more and more pronounced. What is different from other reports is that the pure ABS possessed a nonterminal behavior.[43−45] Münstedt has demonstrated that in rubber-modified polymer melt the yield stress, which was manifested by a plateau in G'-ω plot, resulted from the agglomeration of rubber particles.[46] In addition, the ABS resin here was prepared through copolymerization of styrene and acrylonitrile in the presence of PB particles, so the nonterminal behavior of ABS resin was also related to the interfacial boundaries between the SAN and the PB phase domains.[47,48] In the filled polymer systems, the nonterminal behavior has been attributed to 3D percolated networks.[1,6,22,43,45] Therefore, in our ABS/graphene nanocomposites, the low frequency plateau is the cooperation of the ABS resin itself and the formation of graphene networks in SAN. For the low graphene loading nanocomposites, the solid-like behavior mainly results from the ABS matrix itself, whereas as the graphene content increases to the rheological percolation threshold, which is different from the conductive value previously due to the different distance needed for the percolation phenomenon,[1,6]

graphene networks will form and begin to play an important role. Since the rheological properties in the low frequency regime are regarded to reflect the long-range motion of polymer chains, the nonterminal behavior means that the long-range motion is hindered, resulting in incomplete relaxation of polymer chains. In clay filled systems, the hindrance of clay networks was explained by the physical jamming effect of the dispersed layered silicates with anisotropic disk-like structure.[22,49] Considering that the geometric structure of the graphene nanosheets is similar to that of the clay, the physical jamming effect is proposed to account for the motion retardation. From the TEM micrographs of the 2.33 vol % nanocomposites, graphene nanosheets were randomly dispersed in the continuous SAN phase and 3D networks formed. In the networks, graphene nanosheets are difficult to rotate or tumble freely due to the hindrance of the neighboring ones. Consequently, the motion of polymer chains is restrained in the confined region of the nanosheets, inducing the incomplete relaxation and nonterminal behavior.

Evidence of the formation of the percolated graphene networks can also be seen in Figure 6, where the variation of G' and G'' with frequency was compared for the pure ABS and the nanocomposites containing 0.24 and 2.33 vol % of graphene (nanocomposites of other graphene contents are not shown here for easy reading). It is observed that the G'-ω and G''-ω double-logarithmic plots of pure ABS intersected with each other; but with increasing graphene content, the intersection gradually disappeared. G' became higher than G'' at 0.24 vol % of graphene, and much higher at 2.33 vol %. Larson has clarified the correlation between G' and G'' in typical liquid-like and solid-like materials.[50] For liquid-like behavior, $G' < G''$ is expected, while on the contrary the prospective result $G' > G''$ can be observed for solid-like behavior. Therefore, the growing gap between G'-ω and G''-ω plots with graphene content suggests that the solid-like behavior became more and more prominent, due to the formation and improvement of the graphene networks.

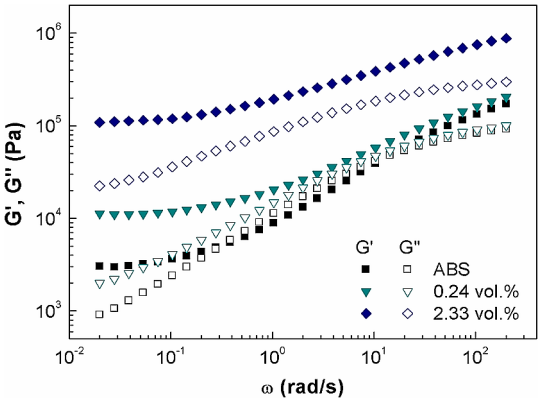

Figure 6. Comparison of storage modulus G' (solid symbols) and loss modulus G'' (hollow symbols) at different graphene loadings.

The effect of graphene nanosheets on the complex viscosity is shown in Figure 7a. The values of complex viscosity increased in the whole frequency range with graphene content, along with more pronounced shear-thinning behavior. Additional insight into the impact of structure evolution with graphene content on the viscoelastic properties can be obtained from the loss tangent, tan δ, where δ is the phase angle. Tan δ is a measure of damping characteristics of the materials. As shown in Figure 7b,

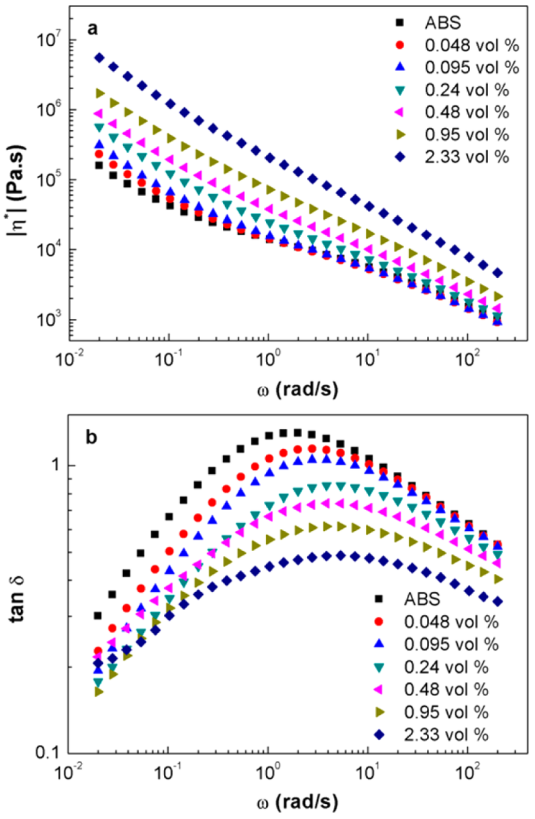

Figure 7. Complex viscosity η^* (a) and loss tangent tan δ (b) of ABS and its graphene nanocomposites as a function of angular frequency ω at 210 °C.

tan δ decreased with graphene content, indicating that the nanocomposites exhibited more solid-like elastic behavior due to the hindrance of graphene networks to energy dissipation.

3.5. Enhancement of Electrical Conductivity by Annealing. The nanocomposites were annealed for varied time at the same condition as compression molding (210 °C, 10 MPa) and the electrical conductivity were measured. As shown in Figure 8, the electrical conductivity of the nanocomposites was enhanced. For example, after 8 h annealing, the electrical conductivity increased by almost 1 order of magnitude from 7.1×10^{-6} to 7.0×10^{-5} S/m for the

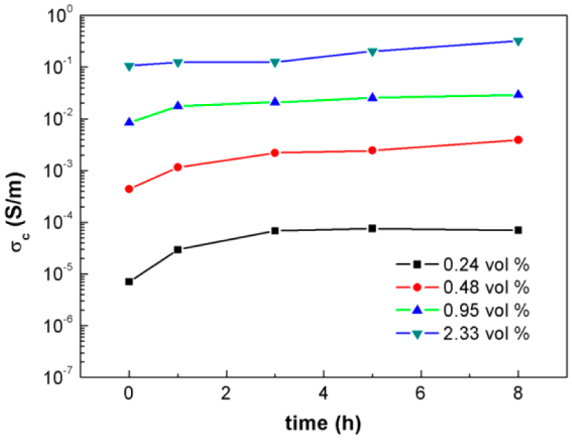

Figure 8. Enhancement of electrical conductivity by annealing treatment as a function of annealing time.

0.24 vol % nanocomposite; for the 0.48, 0.95, and 2.33 vol % nanocomposites, the conductivity increased by 8.9, 3.4, and 2.9 folds, respectively. The increase of electrical conductivity of ABS/graphene nanocomposites can be attributed to the further reduction of graphene and self-improvement of graphene networks during the annealing treatments.

The reduction of graphene oxide by hydrazine hydrate was incomplete, and some oxygen containing groups still existed on the graphene nanosheets. During thermal annealing at high temperature, these groups would undergo thermal degradation, resulting in further reduction. The change of C/O ratio during the annealing treatment was characterized by XPS. As shown in Figure 9, the C/O ratio of the graphene increased from 7.3 to

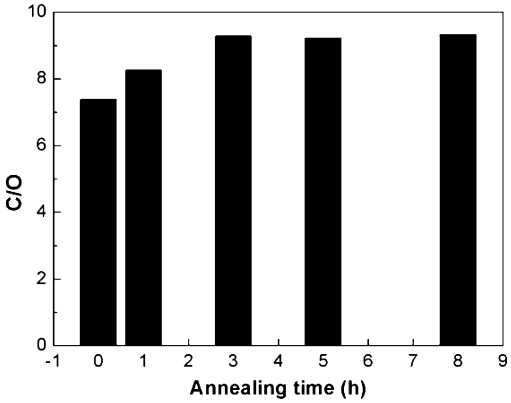

Figure 9. C/O ratio of graphene as a function of annealing time.

8.3 and 9.3 after thermal annealing for 1 and 3 h respectively, while further treatments made no evident impact. The increase of C/O ratio indicates that structure of graphene was further restored during thermal annealing, leading to an increase of electrical conductivity of graphene. As a result, the electrical conductivity of ABS/graphene nanocomposites was enhanced. On the other hand, in CB and CNT filled polymer systems, it has been found that the dispersion of the fillers was not thermodynamically stable.[51−53] The unstable hybrid structure would most likely undergo gelation and network formation rather than macroscopic phase separation at the temperature above the glass transition or melting point of the matrix.[50,53] After annealing treatments, CB particles dispersed in polymer matrix were easy to aggregate and generally form networks during isothermal treatments, hence, several orders of increase in electrical conductivity for polymer/CB composites was made.[51,52] For polymer/CNT systems, electrical conductivity of the composites was also enhanced after annealing treatments, which resulted from further evolution of the CNT networks.[53] Similarly, graphene networks in the polymer matrix was also not in thermodynamic equilibrium state and could be further improved through annealing treatment. Kim et al. reported that the storage modulus of PC/graphene nanocomposites increased with time during dynamic time sweeps, which was attributed to the improvement of graphene networks.[37] Therefore, the thermal reduction of graphene and self-improvement of graphene networks cooperate to benefit the electrical conductivity of ABS/graphene nanocomposites.

As shown in Figure 8, the increase of electrical conductivity by annealing was less pronounced for the nanocomposites with high graphene content, which may arise from the insensitivity of the conductivity to the conductive networks at high loadings. It is well-known that the excess of conductive fillers has little effect on the electrical conductivity when there are sufficient networks for electron transportation. Therefore, though the annealing treatment improved the network structure, it made no striking enhancement to the electrical properties at high loadings.

4. CONCLUSIONS

In an effort to localize graphene nanosheets in SAN phase of ABS, a facile solution coagulation method was used with DMF, a solvent which can dissolve the continuous SAN phase only. The graphene nanosheets were obtained in situ in the solution and thus controlled to reside in SAN phase homogeneously. This dispersion state of graphene nanosheets, united with the extreme geometry, makes it easy to form graphene networks penetrating throughout the polymer matrix. As a result, the nanocomposites displayed an electrical percolation threshold as low as 0.13 vol %. At graphene loading of 0.24 vol %, the electrical conductivity has exceeded the antistatic criterion 10^{-6} S/m. At 2.33 vol %, the conductivity was increased to 0.1 S/m. Similarly, the linear rheological properties of the nanocomposites melt were also influenced obviously by the incorporation of graphene. With increasing graphene content, the melt mechanical modulus and viscosity were enhanced. Under the contribution of the graphene networks, the nanocomposites made a transition to solid-like behavior. Though the graphene networks were established during processing, they were not thermally and thermodynamically stable. Through annealing at 210 °C, graphene nanosheets were further thermally reduced, and the structure of graphene networks was improved. As a result, an enhancement of electrical conductivity was obtained for the annealed nanocomposites.

AUTHOR INFORMATION

Corresponding Author

*Tel./Fax: +86-10-62561945. E-mail: yms@iccas.ac.cn.

Funding

This work was supported by the National Basic Research Program of China (Grant No. 2012CB720304), the "Strategic Priority Research Program" of the Chinese Academy of Sciences (Grant No. XDA09030200), and National Natural Science Foundation of China (Grant No. 51133009).

Notes

The authors declare no competing financial interest.

REFERENCES

(1) Hu, G. J.; Zhao, C. G.; Zhang, S. M.; Yang, M. S.; Wang, Z. G. Low Percolation Thresholds of Electrical Conductivity and Rheology in Poly(Ethylene Terephthalate) through the Networks of Multi-Walled Carbon Nanotubes. *Polymer* **2006**, *47*, 480−488.

(2) Zhang, C.; Yi, X. S.; Yui, H.; Asai, S.; Sumita, M. Morphology and Electrical Properties of Short Carbon Fiber-Filled Polymer Blends: High-Density Polyethylene/Poly (Methyl Methacrylate). *J. Appl. Polym. Sci.* **1998**, *69*, 1813−1819.

(3) Wu, G.; Miura, T.; Asai, S.; Sumita, M. Carbon Black-Loading Induced Phase Fluctuations in PVDF/PMMA Miscible Blends: Dynamic Percolation Measurements. *Polymer* **2001**, *42*, 3271−3279.

(4) Stauffer, D.; Aharony, A. *Introduction to Percolation Theory*, 2nd ed.; Taylor & Francis: London, 2003; pp 89−94.

(5) Nan, C. W.; Shen, Y.; Ma, J. Physical Properties of Composites Near Percolation. *Annu. Rev. Mater. Res.* **2010**, *40*, 131−151.

(6) Du, F. M.; Scogna, R. C.; Zhou, W.; Brand, S.; Fischer, J. E.; Winey, K. I. Nanotube Networks in Polymer Nanocomposites:

Rheology and Electrical Conductivity. *Macromolecules* **2004**, *37*, 9048−9055.
(7) Balberg, I.; Anderson, C. H.; Alexander, S.; Wagner, N. Excluded Volume and Its Relation to the Onset of Percolation. *Phys. Rev. B* **1984**, *30*, 3933−3943.
(8) Balberg, I.; Binenbaum, N.; Wagner, N. Percolation Thresholds in the Three-Dimensional Sticks System. *Phys. Rev. Lett.* **1984**, *52*, 1465−1468.
(9) Charlaix, E. Percolation Threshold of a Random Array of Discs: A Numerical Simulation. *J. Phys. A: Math. Gen.* **1986**, *19*, L533−L536.
(10) Bai, J. B.; Allaoui, A. Effect of the Length and the Aggregate Size of MWNTs on the Improvement Efficiency of the Mechanical and Electrical Properties of Nanocomposites—Experimental Investigation. *Compos. Part A: Appl. Sci.* **2003**, *34*, 689−694.
(11) Li, J.; Ma, P. C.; Chow, W. S.; To, C. K.; Tang, B. Z.; Kim, J. K. Correlations between Percolation Threshold, Dispersion State, and Aspect Ratio of Carbon Nanotubes. *Adv. Funct. Mater.* **2007**, *17*, 3207−3215.
(12) Xu, Z.; Niu, Y.; Wang, Z.; Li, H.; Yang, L.; Qiu, J.; Wang, H. Enhanced Nucleation Rate of Polylactide in Composites Assisted by Surface Acid Oxidized Carbon Nanotubes of Different Aspect Ratios. *ACS Appl. Mater. Inter.* **2011**, *3*, 3744−3753.
(13) Sumita, M.; Sakata, K.; Asai, S.; Miyasaka, K.; Nakagawa, H. Dispersion of Fillers and the Electrical Conductivity of Polymer Blends Filled with Carbon Black. *Polym. Bull.* **1991**, *25*, 265−271.
(14) Gubbels, F.; Jerome, R.; Teyssie, P.; Vanlathem, E.; Deltour, R.; Calderone, A.; Parente, V.; Bredas, J. L. Selective Localization of Carbon Black in Immiscible Polymer Blends: A Useful Tool to Design Electrical Conductive Composites. *Macromolecules* **1994**, *27*, 1972−1974.
(15) Gubbels, F.; Blacher, S.; Vanlathem, E.; Jerome, R.; Deltour, R.; Brouers, F.; Teyssie, P. Design of Electrical Conductive Composites: Key Role of the Morphology on the Electrical Properties of Carbon Black Filled Polymer Blends. *Macromolecules* **1995**, *28*, 1559−1566.
(16) Qi, X. Y.; Yan, D.; Jiang, Z. G.; Cao, Y. K.; Yu, Z. Z.; Fazel, Y.; Nikhil, K. Enhanced Electrical Conductivity in Polystyrene Nanocomposites at Ultra-Low Graphene Content. *Acs Appl. Mater. Inter.* **2011**, *3*, 3130−3133.
(17) Xu, Z.; Zhang, Y.; Wang, Z.; Sun, N.; Li, H. Enhancement of Electrical Conductivity by Changing phase Morphology for Composites Consisting of Polylactide and Poly(epsilon-caprolactone) Filled with Acid-Oxidized Multiwalled Carbon Nanotubes. *ACS Appl. Mater. Inter.* **2011**, *3*, 4858−4864.
(18) Novoselov, K. S.; Geim, A. K.; Morozov, S. V.; Jiang, D.; Zhang, Y.; Dubonos, S. V.; Grigorieva, I. V.; Firsov, A. A. Electric Field Effect in Atomically Thin Carbon Films. *Science* **2004**, *306*, 666−669.
(19) Stankovich, S.; Dikin, D. A.; Dommett, G. H. B.; Kohlhaas, K. M.; Zimney, E. J.; Stach, E. A.; Piner, R. D.; Nguyen, S. T.; Ruoff, R. S. Graphene-Based Composite Materials. *Nature* **2006**, *442*, 282−286.
(20) Zhang, H. B.; Zheng, W. G.; Yan, Q.; Yang, Y.; Wang, J. W.; Lu, Z. H.; Ji, G. Y.; Yu, Z. Z. Electrically Conductive Polyethylene Terephthalate/Graphene Nanocomposites Prepared by Melt Compounding. *Polymer* **2010**, *51*, 1191−1196.
(21) Solomon, M. J.; Almusallam, A. S.; Seefeldt, K. F.; Somwangthanaroj, A.; Varadan, P. Rheology of Polypropylene/Clay Hybrid Materials. *Macromolecules* **2001**, *34*, 1864−1872.
(22) Ren, J. X.; Silva, A. S.; Krishnamoorti, R. Linear Viscoelasticity of Disordered Polystyrene-Polyisoprene Block Copolymer Based Layered-Silicate Nanocomposites. *Macromolecules* **2000**, *33*, 3739−3746.
(23) Kim, H.; Macosko, C. W. Morphology and Properties of Polyester/Exfoliated Graphite Nanocomposites. *Macromolecules* **2008**, *41*, 3317−3327.
(24) Bose, S.; Bhattacharyya, A. R.; Bondre, A. P.; Kulkarni, A. R.; Poetschke, P. Rheology, Electrical Conductivity, and the Phase Behavior of Cocontinuous PA6/ABS Blends with MWNT: Correlating the Aspect Ratio of MWNT with the Percolation Threshold. *J. Polym. Sci., Part A: Polym. Phys.* **2008**, *46*, 1619−1631.
(25) Wu, G.; Li, B.; Jiang, J. Carbon Black Self-Networking Induced Co-Continuity of Immiscible Polymer Blends. *Polymer* **2010**, *51*, 2077−2083.
(26) Hummers, W. S.; Offeman, R. E. Preparation of Graphitic Oxide. *J. Am. Chem. Soc.* **1958**, *80*, 1339−1339.
(27) Li, Y.; Wang, Z. Q.; Yang, L.; Gu, H.; Xue, G. Efficient Coating of Polystyrene Microspheres with Graphene Nanosheets. *Chem. Commun.* **2011**, *47*, 10722−10724.
(28) Viet Hung, P.; Tran Viet, C.; Thanh Truong, D.; Hur, S. H.; Kong, B. S.; Kim, E. J.; Shin, E. W.; Chung, J. S. Superior Conductive Polystyrene − Chemically Converted Graphene Nanocomposite. *J. Mater. Chem.* **2011**, *21*, 11312−11316.
(29) Sachdev, V. K.; Patel, K.; Bhattacharya, S.; Tandon, R. P. Electromagnetic Interference Shielding of Graphite/Acrylonitrile Butadiene Styrene Composites. *J. Appl. Polym. Sci.* **2011**, *120*, 1100−1105.
(30) Ou, R. Q.; Gerhardt, R. A.; Marrett, C.; Moulart, A.; Colton, J. S. Assessment of Percolation and Homogeneity in ABS/Carbon Black Composites by Electrical Measurements. *Compos. Part B: Eng.* **2003**, *34*, 607−614.
(31) Liang, X. Y.; Ling, L. C.; Lu, C. X.; Liu, L. Resistivity of Carbon Fibers/ABS Resin Composites. *Mater. Lett.* **2000**, *43*, 144−147.
(32) Wang, W. Y.; Luo, G. H.; Wei, F.; Luo, J. Electrical Conductivity and Thermal Properties of Acrylonitrile-Butadiene-Styrene Filled with Multiwall Carbon Nanotubes. *Polym. Eng. Sci.* **2009**, *49*, 2144−2149.
(33) Al-Saleh, M. H.; Al-Anid, H. K.; Hussain, Y. A. CNT/ABS Nanocomposites by Solution Processing: Proper Dispersion and Selective Localization for Low Percolation Threshold. *Compos. Part A: Appl. Sci.* **2013**, *46*, 53−59.
(34) Weber, M.; Kamal, M. R. Estimation of the Volume Resistivity of Electrically Conductive Composites. *Polym. Composite* **1997**, *18*, 711−725.
(35) Yoonessi, M.; Gaier, J. R. Highly Conductive Multifunctional Graphene Polycarbonate Nanocomposites. *ACS Nano* **2010**, *4*, 7211−7220.
(36) Chen, G. H.; Weng, W. G.; Wu, D. J.; Wu, C. L. PMMA/Graphite Nanosheets Composite and Its Conducting Properties. *Eur. Polym. J.* **2003**, *39*, 2329−2335.
(37) Kim, H.; Macosko, C. W. Processing-Property Relationships of Polycarbonate/Graphene Composites. *Polymer* **2009**, *50*, 3797−3809.
(38) Shante, V. K. S.; Kirkpatr, S. An Introduction to Percolation Theory. *Adv. Phys.* **1971**, *20*, 325−357.
(39) Cassagnau, P. Payne Effect and Shear Elasticity of Silica-Filled Polymers in Concentrated Solutions and in Molten State. *Polymer* **2003**, *44*, 2455−2462.
(40) Das, A.; Stoeckelhuber, K. W.; Jurk, R.; Saphiannikova, M.; Fritzsche, J.; Lorenz, H.; Klueppel, M.; Heinrich, G. Modified and Unmodified Multiwalled Carbon Nanotubes in High Performance Solution-Styrene-Butadiene and Butadiene Rubber Blends. *Polymer* **2008**, *49*, 5276−5283.
(41) Gauthier, C.; Reynaud, E.; Vassoille, R.; Ladouce-Stelandre, L. Analysis of the Non-Linear Viscoelastic Behaviour of Silica Filled Styrene Butadiene Rubber. *Polymer* **2004**, *45*, 2761−2771.
(42) Hyun, Y. H.; Lim, S. T.; Choi, H. J.; Jhon, M. S. Rheology of Poly(Ethylene Oxide)/Organoclay Nanocomposites. *Macromolecules* **2001**, *34*, 8084−8093.
(43) Lim, S. K.; Hong, E. P.; Song, Y. H.; Park, B. J.; Choi, H. J.; Chin, I. J. Preparation and Interaction Characteristics of Exfoliated ABS/Organoclay Nanocomposite. *Polym. Eng. Sci.* **2010**, *50*, 504−512.
(44) Ma, H. Y.; Tong, L. F.; Xu, Z. B.; Fang, Z. P. Clay Network in ABS-Graft-MAH Nanocomposites: Rheology and Flammability. *Polym. Degrad. Stab.* **2007**, *92*, 1439−1445.
(45) Jiang, L.; Lam, Y. C.; Tam, K. C.; Chua, T. H.; Sim, G. W.; Ang, L. S. Strengthening Acrylonitrile-Butadiene-Styrene (ABS) with Nano-Sized and Micron-Sized Calcium Carbonate. *Polymer* **2005**, *46*, 243−252.
(46) Munstedt, H. Rheology of Rubber-Modified Polymer Melts. *Polym. Eng. Sci.* **1981**, *21*, 259−270.

(47) Niu, Y. H.; Wang, Z. G. Rheologically Determined Phase Diagram and Dynamically Investigated Phase Separation Kinetics of Polyolefin Blends. *Macromolecules* **2006**, *39*, 4175−4183.
(48) Niu, Y. H.; Yang, L.; Shimizu, K.; Pathak, J. A.; Wang, H.; Wang, Z. G. Investigation on Phase Separation Kinetics of Polyolefin Blends through Combination of Viscoelasticity and Morphology. *J. Phys. Chem. B* **2009**, *113*, 8820−8827.
(49) Wang, K.; Liang, S.; Deng, J. N.; Yang, H.; Zhang, Q.; Fu, Q.; Dong, X.; Wang, D. J.; Han, C. C. The Role of Clay Network on Macromolecular Chain Mobility and Relaxation in Isotactic Polypropylene/Organoclay Nanocomposites. *Polymer* **2006**, *47*, 7131−7144.
(50) Larson, R. G. *The Structure and Rheology of Complex Fluids*; Oxford University Press: New York, 1999; pp 13−15, 334−337, 281, 291−297.
(51) Cao, Q.; Song, Y. H.; Tan, Y. Q.; Zheng, Q. Thermal-Induced Percolation in High-Density Polyethylene/Carbon Black Composites. *Polymer* **2009**, *50*, 6350−6356.
(52) Wu, G. Z.; Asai, S.; Sumita, M. Carbon Black as a Self-Diagnosing Probe to Trace Polymer Dynamics in Highly Filled Compositions. *Macromolecules* **2002**, *35*, 1708−1713.
(53) Li, W. L.; Zhang, Y. Q.; Yang, J. J.; Zhang, J.; Niu, Y. H.; Wang, Z. G. Thermal Annealing Induced Enhancements of Electrical Conductivities and Mechanism for Multiwalled Carbon Nanotubes Filled Poly(Ethylene-co-Hexene) Composites. *ACS Appl. Mater. Inter.* **2012**, *4*, 6468−6478.